

# A simple mechanism for the enhancement of the inflationary power spectrum

I. Dalianis<sup>1</sup>, A. Katsis<sup>2</sup> and N. Tetradis<sup>2</sup>

<sup>1</sup>Department of Physics, University of Cyprus, Nicosia 1678, Cyprus

<sup>2</sup>National and Kapodistrian University of Athens, Zographou 15784, Greece

E-mail: [ntalianis.ioannis@ucy.ac.cy](mailto:ntalianis.ioannis@ucy.ac.cy), [ariskatsis@phys.uoa.gr](mailto:ariskatsis@phys.uoa.gr), [ntetrad@phys.uoa.gr](mailto:ntetrad@phys.uoa.gr)

**Abstract.** The background evolution in two-field inflation can feature two distinct stages, corresponding to the evolution along two successive field directions. When the second stage occurs at a significantly lower energy scale, the inflationary trajectory includes a sharp transition, accompanied by a series of rapid turns in field space. Fluctuations crossing the Hubble horizon during this turning phase can experience amplification by several orders of magnitude. This mechanism is very intuitive and can be implemented even in simple two-field models. It produces a peak in the scalar power spectrum that can lead to significant abundances of primordial black holes and secondary gravitational waves.

---

## Contents

<b>1</b>	<b>Introduction</b>	<b>1</b>
<b>2</b>	<b>Assisted enhancement from the transition between two inflationary plateaux</b>	<b>3</b>
2.1	The inflationary evolution of the background and fluctuations	3
2.2	A simple scenario of assisted enhancement	5
2.3	The dependence on the parameters of the model	8
<b>3</b>	<b>The relevance of the mechanism for general two-field models</b>	<b>9</b>
<b>4</b>	<b>Gravitational waves and primordial black holes</b>	<b>9</b>
4.1	Non-Gaussianities	10
4.2	Primordial Black Holes and Observational Constraints	11
4.3	Scalar-induced stochastic gravitational waves	11
<b>5</b>	<b>Conclusions and outlook</b>	<b>12</b>

---

## 1 Introduction

Inflationary potentials with special structure can induce significant departures from scale invariance in the primordial spectrum of curvature perturbations  $\mathcal{R}$ . Such deviations may be confined to length scales far smaller than those directly constrained by cosmic microwave background (CMB) observations, thus leaving large-scale observables unaffected while enhancing power on small scales. This possibility is particularly important because perturbations generated during the later stages of inflation correspond to wavelengths well below those imprinted on the CMB sky and are therefore only weakly constrained by current cosmological data [1]. Nevertheless, a strong amplification of the curvature spectrum on such scales may have striking phenomenological consequences, including the generation of a stochastic background of gravitational waves (GWs) sourced at second order by scalar perturbations [2–4] and the formation of primordial black holes (PBHs) [5–8]. These signatures provide a powerful observational portal into inflationary physics far beyond the CMB window.

Multi-field inflation provides a natural and well-established framework in which localized enhancement of  $\mathcal{R}$  can arise dynamically. Non-trivial trajectories in field space, such as bends or turns, are generic in the presence of multiple scalar degrees of freedom and potentials with curved directions [9–20]. Whenever the inflationary trajectory undergoes a turn, isocurvature (entropic) perturbations can efficiently source the adiabatic curvature mode, leading to super-horizon evolution of  $\mathcal{R}$  [9, 10, 13, 21–25]. A significant amplification takes place if during the sharp turn the isocurvature modes experience a transition from heavy to light. This sourcing mechanism opens up a wide range of possibilities for generating sharp features and localized peaks in the curvature power spectrum without violating observational constraints on large scales [17–19, 26–35].

Strong and localized enhancements of the curvature power spectrum can arise through the constructive superposition of multiple transient features in the background evolution, both in single-field inflation [36, 37] and in two-field inflation [38], see also Ref. [39] for a concise review. In particular, Ref. [38] showed that sharp turns in field space can act as brief

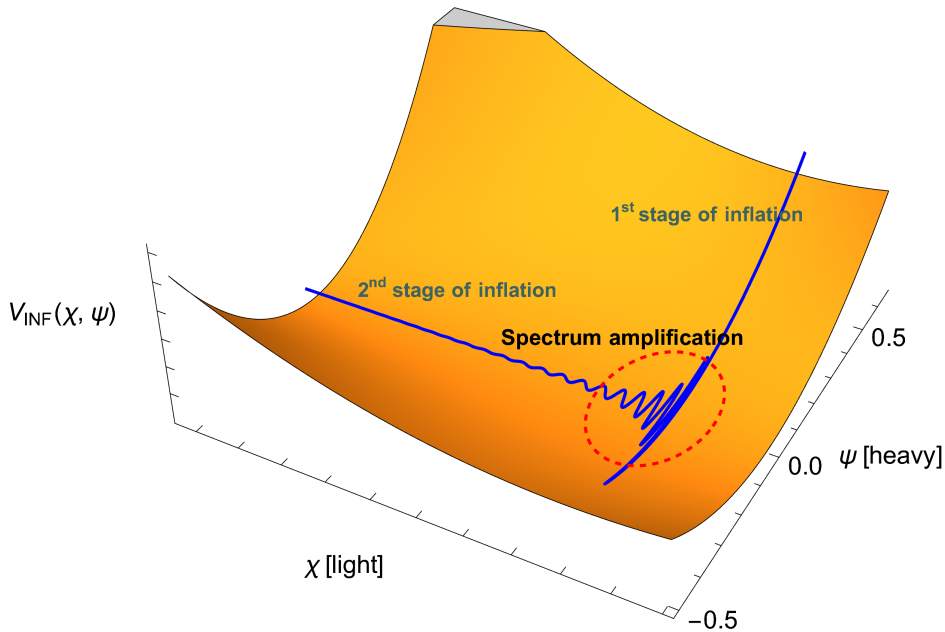


**Figure 1:** A schematic illustration of the proposed minimal mechanism, showing the qualitative shape of the inflationary potential and the corresponding field-space trajectory, with a zoom into the transition region. The two stages of inflation are indicated in the plot.

but efficient sources for the curvature perturbation, leading to resonant growth when several such events occur within a small number of efoldings. Remarkably, this enhancement can take place even for canonical kinetic terms and a flat field-space metric, provided the trajectory experiences repeated bending. An explicit realization of this general mechanism was later constructed in Ref. [40], where a simple class of two-field potentials was shown to exhibit successive turns along a sinusoidal valley. In this setup, a controlled interaction between the scalar fields dynamically carves out a turning trajectory in field space, effectively upgrading otherwise standard single-field models into two-field scenarios with additional phenomenological properties [13, 40]. The enhancement of the curvature spectrum was characterized as “assisted” in Ref. [40] because it results through the influence of the isocurvature perturbations that arise temporarily during the turns.

In this work, we argue that qualitatively similar behavior can emerge even in the absence of finely tuned or explicitly engineered features in the inflationary potential. As we will demonstrate, the geometry of field-space trajectories in relatively simple two-field models can naturally mimic the enhancement mechanisms previously associated with more elaborate constructions. We will show that the key ingredients are an intermediate oscillatory regime and a significant separation between the energy scales of the two inflationary plateaux. This observation considerably broadens the class of inflationary models capable of generating large small-scale curvature perturbations.

We present the underlying mechanism within a minimal two-field inflationary setup featuring canonical kinetic terms and a simple interaction potential. The inflationary dynamics unfolds in two stages: an initial phase at a higher energy scale that fixes the CMB normalization, followed by a second stage at a lower energy scale. As the system transitions between these stages, the heavier field undergoes damped oscillations, which induce repeated turns in

the background trajectory in field space. These turns act as transient sources for the curvature perturbation, leading to a localized amplification of the power spectrum over a narrow range of scales. An illustration of this mechanism is displayed in Fig. 1.

The resulting enhancement has direct and testable implications for PBH formation, the generation of scalar-induced gravitational waves (SIGWs), and the appearance of non-Gaussian signatures at the relevant small scales. In particular, the associated SIGW background can fall within the sensitivity ranges of pulsar timing array experiments as well as future space-based gravitational wave interferometers.

We discuss the mechanism of “assisted enhancement” in Section 2. We summarize the basic formalism for two-field inflation in Subsection 2.1 and study a simple mode that realizes the mechanism in Subsection 2.2. We analyze the dependence of the power spectrum on the parameters of the model that control the evolution of the background and fluctuations in Subsection 2.3. We comment on how this mechanism may appear in more general inflationary scenarios in Section 3. The phenomenological implications for gravitational waves and PBHs are studied in Section 4. We present our conclusion in Section 5. Throughout the paper we express all dimensionful quantities in units of  $M_{\text{Pl}}$ , suppressing factors of  $M_{\text{Pl}}$  for notational simplicity.

## 2 Assisted enhancement from the transition between two inflationary plateaux

### 2.1 The inflationary evolution of the background and fluctuations

We consider a simple action of two scalar fields,  $\vec{\phi} = (\chi, \psi)$ , with canonical kinetic terms, interacting through the potential  $V(\chi, \psi)$ :

$$S = \int d^4x \sqrt{-g} \left[ \frac{R}{2} - \frac{1}{2} g^{\mu\nu} \partial_\mu \chi \partial_\nu \chi - \frac{1}{2} g^{\mu\nu} \partial_\mu \psi \partial_\nu \psi - V(\chi, \psi) \right]. \quad (2.1)$$

in a flat FRW metric. We measure time in terms of efoldings of expansion. We also rotate the field-space axes and parametrize with respect to the directions tangent and normal to the trajectory in field space [10]. The basic elements of the inflationary evolution in our notation are already described in [13, 25, 40]. The background evolves as

$$\chi_{,NN} + \left( 3 + \frac{H_{,N}}{H} \right) \chi_{,N} + \frac{V_{,\chi}}{H^2} = 0 \quad (2.2a)$$

$$\psi_{,NN} + \left( 3 + \frac{H_{,N}}{H} \right) \psi_{,N} + \frac{V_{,\psi}}{H^2} = 0 \quad (2.2b)$$

$$\frac{2V}{6 - (\chi_{,N}^2 + \psi_{,N}^2)} = H^2. \quad (2.2c)$$

The parameter  $\eta$  is also decomposed into its projections along these newly defined orientations

$$\epsilon = \frac{1}{2} (\chi_{,N}^2 + \psi_{,N}^2), \quad (2.3)$$

$$\eta_{\parallel} = 3 + \frac{V_{,\chi} \chi_{,N} + V_{,\psi} \psi_{,N}}{H^2 (\chi_{,N}^2 + \psi_{,N}^2)}, \quad (2.4)$$

$$\eta_{\perp} = \frac{V_{,\chi} \psi_{,N} - V_{,\psi} \chi_{,N}}{H^2 (\chi_{,N}^2 + \psi_{,N}^2)}. \quad (2.5)$$

The parameter  $\eta_{\parallel}$  is equivalent to the standard second slow-roll parameter of single-field inflation, while  $\eta_{\perp}$  parametrizes the turning rate of the trajectory in field space.

We describe fluctuations from the classical trajectory in terms of the curvature and isocurvature fields,  $\mathcal{R}$  and  $\mathcal{F} = \sqrt{2\epsilon}\mathcal{S}$  respectively [10, 13, 25, 41–43]. The spectrum of the fluctuations is determined by the Mukhanov-Sasaki coupled evolution

$$\mathcal{R}_{k,NN} + r_1(N)\mathcal{R}_{k,N} + r_2(N)k^2\mathcal{R}_k = -r_3(N)\mathcal{F}_{k,N} - r_4(N)\mathcal{F}_k, \quad (2.6a)$$

$$\mathcal{F}_{k,NN} + s_1(N)\mathcal{F}_{k,N} + (s_4(N) + r_2(N)k^2)\mathcal{F}_k = s_3(N)\mathcal{R}_{k,N}, \quad (2.6b)$$

where  $\mathcal{R}_k$  and  $\mathcal{F}_k$  are Fourier-transformed quantities and everything is expressed in terms of efoldings  $N$ . The power distributed to each mode can be deduced by squaring the amplitude of the corresponding fluctuation:

$$\mathcal{P}_{\mathcal{R}}(k) = \frac{k^3}{2\pi^2}|\mathcal{R}_k|^2, \quad (2.7a)$$

$$\mathcal{P}_{\mathcal{F}}(k) = \frac{k^3}{2\pi^2}|\mathcal{F}_k|^2. \quad (2.7b)$$

The explicit formulas for the evolution coefficients are:

$$r_1 \equiv 3 + \epsilon - 2\eta_{\parallel}, \quad r_2 \equiv \frac{e^{-2N}}{H^2}, \quad r_3 \equiv 2\frac{\eta_{\perp}}{\sqrt{2\epsilon}}, \quad r_4 \equiv 2\frac{\eta_{\perp}}{\sqrt{2\epsilon}}\left(3 - \eta_{\parallel} + \frac{\eta_{\perp,N}}{\eta_{\perp}}\right) \quad (2.8a)$$

$$s_1 \equiv 3 - \epsilon, \quad s_3 \equiv 2\sqrt{2\epsilon}\eta_{\perp}, \quad s_4 \equiv (\mu/H)^2 - \eta_{\perp}, \quad (2.8b)$$

A useful quantity that we employ as a background-level precursor of enhancement is

$$W \equiv (\eta_{\perp})^2 - (\mu/H)^2 = -(M_{\text{eff}}/H)^2, \quad (2.9)$$

where  $\mu$  is the bare mass of the fluctuation orthogonal to the background trajectory, given by

$$\mu^2 \equiv N_{\chi}N_{\chi}V_{,\chi\chi} + N_{\psi}N_{\psi}V_{,\psi\psi} + 2N_{\chi}N_{\psi}V_{,\chi\psi}, \quad (2.10)$$

with

$$N_{\chi} = \frac{\dot{\psi}}{\sqrt{\dot{\chi}^2 + \dot{\psi}^2}}, \quad N_{\psi} = -\frac{\dot{\chi}}{\sqrt{\dot{\chi}^2 + \dot{\psi}^2}}. \quad (2.11)$$

The parameter  $M_{\text{eff}}^2$  corresponds to the coefficient of the  $\mathcal{F}^2$  term in the expansion of the action, which can be interpreted as the effective mass term of the fluctuation [13].

The mechanism of assisted enhancement can be summarized as follows<sup>1</sup>: The bending of the trajectory is encoded in the turning parameter  $\eta_{\perp}$  and is determined by the background evolution. During the bending, a pulse of positive  $W$  is generated that transiently drives  $M_{\text{eff}}^2$  tachyonic, leading to the exponential growth of isocurvature perturbations. The adiabatic mode responds to this increase because it is coupled to the isocurvature one through the turning parameter [44]. Later, when the turn or series of turns is completed, the isocurvature mode decays but the amplitude of the adiabatic mode freezes at an increased value.

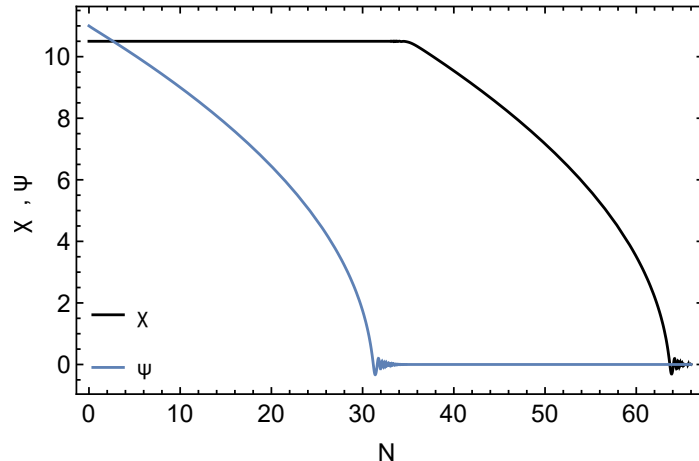


**Figure 2:** The background solutions for  $\chi(N)$  (black) and  $\psi(N)$  (blue) for the model (2.12) with parameters  $m_\chi^2 = 8 \times 10^{-12}$ ,  $m_\psi^2 = 4 \times 10^{-7}$  and  $c_w = 4 \times 10^{-3}$ .

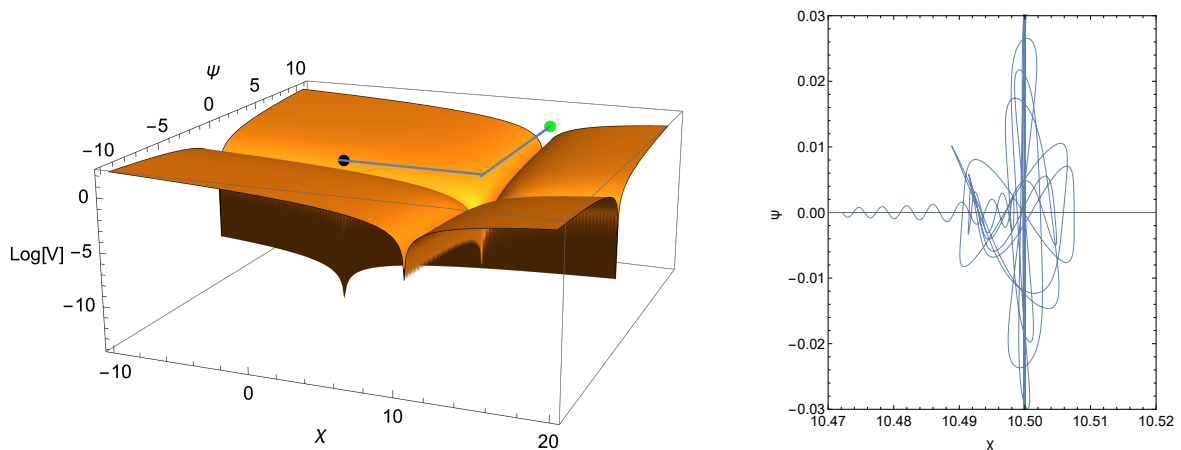


**Figure 3:** Left panel: The field trajectory shown on a logarithmic scale for the potential (2.12), highlighting its evolution across different energy scales. Right panel: A zoomed-in view of the trajectory in field space during the transition stage, highlighting the multiple turns that characterize the two-field dynamics. Both axes are in Planck units.

## 2.2 A simple scenario of assisted enhancement

When considering the background evolution equations (2.2) it becomes apparent that the problem is analogous to a ball travelling on a two-dimensional  $(\chi, \psi)$  terrain with height  $V(\chi, \psi)$  and friction encoded in  $H$ . The crucial observation is that one does not have to carve a snaking valley in the potential in order to generate a trajectory with successive turns. Even for the inside of a tilted cylinder, if we place the ball at some random position away from the tilted valley which we take in the  $\chi$  direction, the ball will naturally oscillate (with decaying amplitude) in the perpendicular  $\psi$  direction, while also moving down the valley. This type of evolution can take place in two-field models at the end of inflation before or during reheating. On the other hand, we argue here that it can also arise during the stage

<sup>1</sup>See [40] for a more detailed analysis.

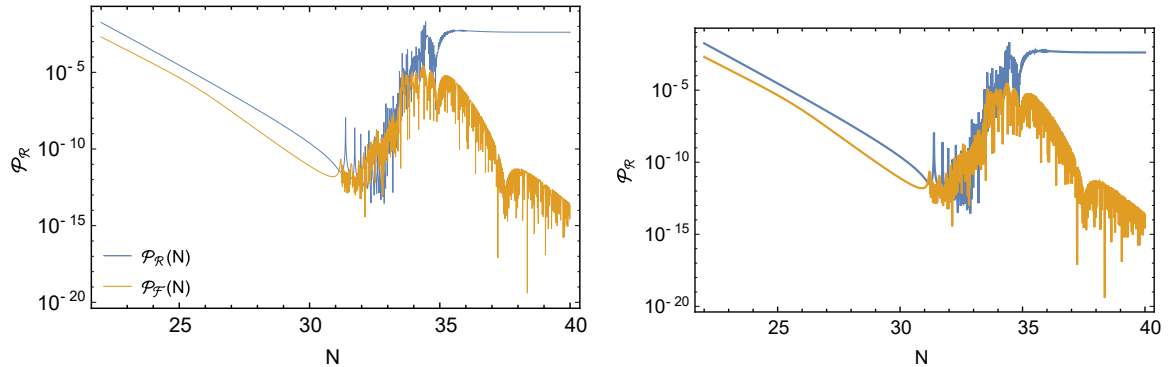


**Figure 4:** Left panel: The evolution of the parameter  $W$  defined in (2.9). It is negative during the first stage of evolution, while large positive pulses occur during the transition stage. Right panel: For the Fourier mode  $k_p = 7.6 \times 10^{10} \text{ Mpc}^{-1}$  we plot  $\mathcal{P}_{\mathcal{R}}(N)$  (blue) and  $\mathcal{P}_{\mathcal{F}}(N)$  (yellow) for the same model.

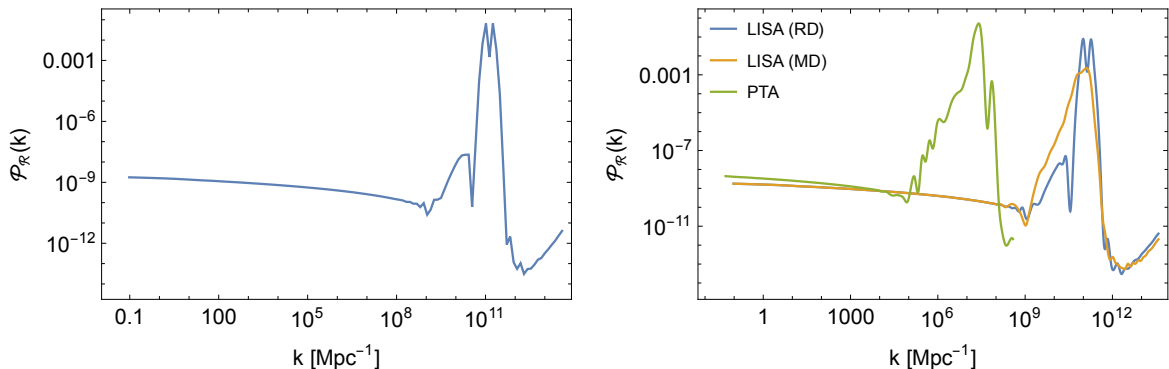


**Figure 5:** Left panel: A representative shape of the scalar power spectrum. Right panel: Three power spectra whose phenomenological implications for GWs and PBHs are discussed in Section 4.

of evolution between two inflationary plateaux, when the vacuum energy is substantial. If the shape of the potential is such that the turns in field space are sharp, the spectrum of fluctuations around the background trajectory can be strongly enhanced.

In order to confirm that this scenario does not require elaborate model building, we consider here a simple potential that will serve as our reference model throughout the rest of the paper:

$$V(\chi, \psi) = m_\chi^2 \chi^2 + m_\psi^2 \psi^2 + c_w \psi^2 (\chi - \chi_0)^2 . \quad (2.12)$$

This potential features two valleys, located at  $\psi = 0$  and  $\chi = \chi_0$ . If the system initially starts with  $|\psi| > 0$ , the field  $\psi$  slowly rolls along the valley near  $\chi = \chi_0$ . During this first stage, the inflationary energy density is dominated by the contribution  $m_\psi^2 \psi^2$ . As  $\psi$  approaches the lowest point of the first valley, it begins to oscillate around  $\psi = 0$ . At the same time the field configuration gradually transitions into the second valley at  $\psi = 0$ , where the second and final stage of inflation takes place with the energy density dominated by the term  $m_\chi^2 \chi^2$ . A schematic presentation of the field evolution is given in Fig. 1.

For a more precise discussion, we focus on an explicit example with benchmark param-

eters. The masses are chosen as  $m_\chi^2 = 8 \times 10^{-12}$  and  $m_\psi^2 = 4 \times 10^{-7}$ , with an interaction constant  $c_w = 4 \times 10^{-3}$ . The evolution starts at  $N = 0$  from the initial field values  $(\chi_0, \psi_0) = (10.5, 11)$ . Figure 2 shows the resulting background evolution for this benchmark configuration. It consists of two inflationary stages, approximately one in each field direction, and a brief intermediate phase during which inflation is interrupted. During the first stage the heavier field  $\psi$  makes its descent towards  $\psi = 0$ , while the lighter field  $\chi$  is frozen at the value  $\chi = \chi_0$ . When  $\psi$  approaches its minimum value  $\psi = 0$  at an intermediate time  $N \simeq 31$ , it begins to oscillate about this point until approximately  $N \simeq 36$ . This short interval of a few efoldings constitutes the transition stage. When the amplitude of the  $\psi$  oscillations drops sufficiently, the system enters the second stage of inflation, during which  $\chi$  slowly rolls toward the absolute minimum of the potential. The true vacuum, where reheating is expected to take place, is reached at  $N \simeq 65$  and corresponds to  $(\chi, \psi) = (0, 0)$ . For different choices of model parameters, the duration of inflation and the corresponding efoldings can vary, allowing for a smaller or larger total value of  $N$  to be realized. We also point out that an additional initial stage is possible if the system does not start exactly on the first valley of the potential. This is brief, as the effective friction quickly forces the system into a slow-roll evolution along the first valley.

GW probe	$m_\chi^2$	$m_\psi^2$	$c_w$	$\chi_0$	$\psi_0$
PTA	$3.2 \times 10^{-11}$	$1.0 \times 10^{-6}$	0.01	12.0	9.3
LISA (RD)	$8.0 \times 10^{-12}$	$4.0 \times 10^{-7}$	0.004	10.5	11.0
LISA (MD)	$3.16 \times 10^{-11}$	$4.0 \times 10^{-7}$	0.004	8.0	11.0

**Table 1:** Model parameters, in Planck units, for the potential (2.12) and scenarios relevant for the PTA and LISA frequency bands.

In the left panel of Fig. 3 we show the potential on a logarithmic scale in order to make the slopes visible, with the field trajectory overlaid. A zoomed-in view of the trajectory during the transition stage is shown in the right panel. For  $31 < N < 33$  there are large oscillations in the  $\psi$  axis while  $\chi$  remains at  $\chi_0$ . For  $33 < N < 34$ , strong turns in field space take place that display a similarity with Lissajous curves. For  $34 < N < 35$ , the trajectory moves from  $\chi_0$  towards the minimum in a sine-type curve, involving many smaller turns in field space. In the left panel of Fig. 4 we depict the parameter  $W$  defined in (2.9). It is strictly negative during the first stage. On the other hand, the oscillations during the transition between the two stages produce a series of pulses of positive  $W$ . These pulses render the isocurvature fluctuations unstable. In the right panel of Fig. 4 we show the evolution of the amplitude of the isocurvature (yellow) and adiabatic (blue) fluctuations for  $k_p = 7.6 \times 10^{10} \text{ Mpc}^{-1}$ . When the pulses of positive  $W$  occur, both isocurvature and adiabatic amplitudes increase in a series of small steps. Then the isocurvature amplitude decays and the adiabatic amplitude freezes at a value increased by 7 orders of magnitude. In the left panel of Fig. 5 we present the numerical results for the curvature power spectrum  $\mathcal{P}_{\mathcal{R}}$ . A relatively narrow peak appears around  $k_p$ , while the amplitude remains at the familiar  $A_s$  value around  $k_* = 0.05 \text{ Mpc}^{-1}$ . In the right panel we present this spectrum together with two additional ones, corresponding to parameter choices different from the benchmark configuration. The corresponding parameter values are listed in Table 1. Their phenomenological implications are discussed in Section 4 and are illustrated in Fig. 7.

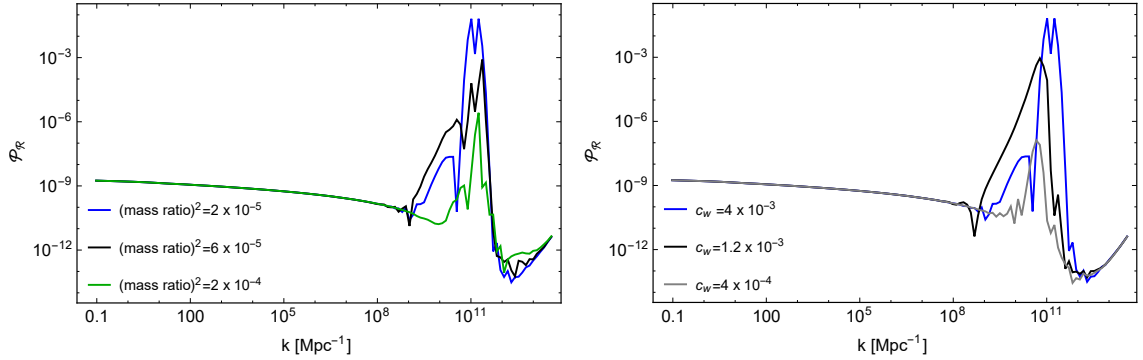


**Figure 6:** The scalar power spectrum of the adiabatic perturbation,  $\mathcal{P}_{\mathcal{R}}(k)$ , for the band of Fourier modes  $0.01 \text{ Mpc}^{-1} \leq k \leq 10^{14} \text{ Mpc}^{-1}$  at  $N = 40$ . In each panel we depict its variation as we change one parameter. Left: mass ratio  $(m_{\chi}/m_{\psi})^2 = 2 \times 10^{-5}$  (blue),  $2 \times 10^{-4}$  (green),  $6 \times 10^{-5}$  (black). Right: interaction strength  $c_w = 4 \times 10^{-3}$  (blue),  $1.2 \times 10^{-3}$  (black),  $4 \times 10^{-4}$  (grey).

### 2.3 The dependence on the parameters of the model

The features of the power spectrum of fluctuations have an intuitive and rather simple dependence on the parameter choices for the inflationary model.

1. The mass hierarchy  $m_{\psi}/m_{\chi}$  dictates the difference in the energy levels of the two inflationary stages. For a larger hierarchy we expect a sharper drop from the plateau of the first stage to the much lower plateau of the second stage. This generates more numerous and also sharper turns in field space during the intermediate stage, which lasts until the original energy density is depleted through the effective friction term in the evolution equations. Ultimately, this leads to a larger enhancement of the power spectrum. This behavior is apparent in the left panel of Fig. 6.
2. The interaction term controls the steepness of the walls around the valley in which the initial part of the field trajectory takes place. The convexity of the potential is determined by  $c_w \psi^2$ , inducing a large mass term for the  $\chi$  fluctuations that act as the isocurvature modes during this stage. As a result, these modes do not become significant and the spectrum around the CMB scales is typical of single-field inflation. The walls around  $\chi_0$  are lowered at  $\psi = 0$ , allowing the evolution to continue along the  $\chi$  direction eventually. Large values of  $c_w$  reduce the size of the window towards the second valley of the potential, so that the fields get trapped for a longer period around the point  $(\chi_0, 0)$ . This results in the evolution depicted in the right panel of Fig. 3 with a large number of turns. Both curvature and isocurvature modes are activated during this stage, resulting in the enhancement of the power spectrum. This behavior is apparent in the right panel of Fig. 6, which demonstrates that a larger value of  $c_w$  increases the enhancement of the spectrum.
3. The value of  $\psi_0$ , which can be interpreted as denoting the point at which the fields settle on the first valley of the potential after some initial evolution, determines the duration of the first inflationary stage. Thus, it fixes the number of efoldings  $\Delta N_1 = N_p - N_*$  between the time  $N_*$  that the CMB scales cross the horizon and the time  $N_p$  of the

transition to the second inflationary stage. Similarly,  $\chi_0$  controls the duration of the second stage  $\Delta N_2 = N_{\text{end}} - N_p$ , and thus the total number of efoldings.

### 3 The relevance of the mechanism for general two-field models

Our discussion of the mechanism of enhancement was carried out with the simple potential (2.12). The main ingredients of our scenario are the two inflationary stages taking place on two plateaux along two straight directions of the potential, and an intermediate stage during which the fields are trapped around the intersection of the two directions. The mass terms, which are parts of any two-field potential, are the simplest means to control the ratio of the energy scales characterizing the two plateaux. A large hierarchy between them implies that the more massive field ( $\psi$  in our scenario) has large kinetic energy after the end of the first inflationary stage, of the order of the vacuum energy during this stage. If the vacuum energy of the second inflationary stage is much lower than that of the first one, it takes long for the kinetic energy to be depleted by the effective friction term. Thus the system stays in the intermediate stage for an extended period of time. The numerous turns that take place before the slow-roll evolution of the lighter field ( $\chi$  in our scenario) sets in lead to a localized enhancement of the power spectrum.

We expect that this type of enhancement is generically present in two- and multi-field inflation, and can arise for a broad range of potential shapes, including different plateau structures and interaction terms. The essential requirement is a hierarchy between the energy scales of the two inflationary stages, together with parameters that allow for a transition regime with repeated turns in the background trajectory. The model considered above can be readily reformulated or generalized, as long as the above essential ingredients are present. For example, additional higher-order terms or deformations can be included in any field direction. Such modifications of the potential during the first stage may be necessary in order to adjust the observables at CMB scales, such as the spectral index, to the experimentally deduced values, without spoiling the small-scale enhancement of the spectrum.

More generally, the mechanism can be viewed as a consequence of the transient excitation of entropic fluctuations during the transition stage. Successive turns efficiently transfer power from isocurvature to curvature modes, leading to a localized enhancement of  $\mathcal{P}_{\mathcal{R}}(k)$  without the need for fine-tuned features. From this perspective, the detailed functional form of the potential is secondary. Assisted enhancement should therefore be a generic possibility in a wide class of multi-field models motivated by effective field theory or supergravity. For example, we have verified that similar behavior occurs for potentials involving hyperbolic tangent terms, such as

$$V(\chi, \psi) = c_\chi \tanh^2(\chi - \chi_1) + c_\psi \tanh^2(\psi) + c_w \psi^2 \tanh^2(\chi - \chi_0). \quad (3.1)$$

Such structures commonly appear in supergravity constructions [45, 46] and cosmological attractor models [47, 48], while couplings of this type also arise in inflationary scenarios with non-minimal interactions with gravity [49–51].

### 4 Gravitational waves and primordial black holes

Significant effort is currently being devoted to the detection of gravitational waves across a wide range of frequencies. Ground-based interferometers such as LIGO-Virgo-KAGRA (LVK) have established GW astronomy through compact binary mergers, while pulsar timing array

(PTA) collaborations, including NANOGrav and the IPTA, have reported strong evidence for a nanohertz stochastic gravitational wave background with Hellings–Downs-like correlations [52–56]. Future space-based missions such as LISA will probe the complementary millihertz band, together with next generation terrestrial detectors bridging PTA and ground-based sensitivities [57, 58].

While many GW signals originate from late-time astrophysical sources, an especially intriguing possibility is a primordial contribution from the early Universe [59, 60]. Scalar perturbations generated during inflation inevitably source gravitational waves at second order, but in minimal slow-roll models the resulting signal is unobservably small. However, inflationary scenarios with localized enhancements of the curvature power spectrum, such as those produced by the sequences of turns in multi-field trajectories discussed here, can generate a strong stochastic background upon horizon reentry, potentially accompanied by PBH formation [61–65].

The scale of the enhancement can be parameterized by the number of efoldings after the CMB pivot scale  $k_* = 0.05 \text{ Mpc}^{-1}$  exits the horizon. A peak at  $k_p \simeq 0.38 \times 10^P \text{ Mpc}^{-1}$  corresponds to

$$N_p - N_* \simeq \ln\left(\frac{k_p}{k_*}\right) \simeq 2 + 2.3 P. \quad (4.1)$$

Features appearing  $\sim 16$  efoldings after CMB horizon exit lead to scalar-induced gravitational waves (SIGWs) in the nanohertz PTA band, while  $\sim 30$  efoldings correspond to millihertz frequencies targeted by LISA. The associated mapping between frequency, comoving scale, and characteristic PBH mass is approximately

$$k \simeq 6 \times 10^5 \left(\frac{f}{10^{-9} \text{ Hz}}\right) \text{ Mpc}^{-1}, \quad M_H \simeq 33 \left(\frac{10^{-9} \text{ Hz}}{f}\right)^2 M_\odot. \quad (4.2)$$

Thus, PTA frequencies are naturally linked to solar-mass PBHs, whereas LISA frequencies correspond to sublunar or asteroid-mass PBHs, mass windows that are among the least constrained and may allow PBHs to constitute a significant fraction of the dark matter [66, 67].

#### 4.1 Non-Gaussianities

The enhancement mechanism discussed in this work relies on repeated turns of the inflationary trajectory in field space, which generically induce superhorizon evolution of the comoving curvature perturbation  $\mathcal{R}$  through its coupling to entropic modes. Periods of rapid turning not only amplify the scalar power spectrum but also inevitably generate non-Gaussian curvature perturbations via nonlinear entropic–adiabatic interactions. In the effective single-field description, applicable during strong turns, the adiabatic mode propagates with a reduced sound speed, leading to equilateral-type non-Gaussianity with amplitude  $f_{\text{NL}}^{\text{equil}} \sim \mathcal{O}(c_s^{-2})$  [41, 68].

In the scenarios considered here, the turning dynamics is localized in e-folding time during the brief transition between two inflationary stages. Consequently, both the enhancement of the curvature power spectrum  $\mathcal{P}_{\mathcal{R}}(k)$  and the associated non-Gaussianities are strongly scale dependent, affecting only modes exiting the horizon near the peak scale  $k_p$ . We expect that CMB-scale modes remain essentially unaffected and continue to satisfy current observational constraints [69].

Despite this localization, non-Gaussian corrections enter exponentially in the PBH formation probability. As a result, even moderate values  $f_{\text{NL}}^{\text{loc}} = \mathcal{O}(1)$  can change the predicted

PBH abundance by several orders of magnitude [70, 71]. Non-Gaussianity can also modify the amplitude and spectral shape of SIGWs [72]. A dedicated treatment of these effects is therefore essential for precision PBH predictions, but lies beyond the scope of the present work.

## 4.2 Primordial Black Holes and Observational Constraints

Assuming Gaussian primordial perturbations and approximately spherical collapse, the fraction of the Universe collapsing into PBHs during radiation domination is

$$\beta(M) = \int_{\delta_c}^{\infty} \frac{d\delta}{\sqrt{2\pi\sigma^2(M)}} \exp\left(-\frac{\delta^2}{2\sigma^2(M)}\right) \simeq \frac{1}{2} \operatorname{erfc}\left(\frac{\delta_c}{\sqrt{2}\sigma(M)}\right), \quad (4.3)$$

where  $\sigma(M)$  is the variance of the density contrast and  $\delta_c$  is the collapse threshold. Since  $\beta(M)$  depends exponentially on  $\delta_c$ , PBH abundance predictions are extremely sensitive to its value. The threshold is not universal [73–76] and is typically treated as an effective parameter in the range  $\delta_c \sim 0.3$ – $0.5$ .

The present-day PBH dark matter fraction,  $f_{\text{PBH}}(M) \equiv \Omega_{\text{PBH}}(M)/\Omega_{\text{DM}}$ , is proportional to  $\beta(M)$ . Consequently, the predicted abundance is also highly sensitive to primordial non-Gaussianities, since PBH formation probes the extreme tail of the probability distribution [70, 71, 77–80].

PBHs may alternatively form during an early matter-dominated era, as could occur for sufficiently late reheating. In this case the collapse fraction scales polynomially with the variance [81, 82],

$$\beta(\sigma) = 0.056 \sigma^5, \quad (4.4)$$

implying a significantly reduced sensitivity to non-Gaussian corrections.

Across most of the PBH mass spectrum, stringent bounds constrain the allowed fraction of dark matter in PBHs [7, 83, 84]. The weakest constraints occur in the window  $M_{\text{PBH}} \sim 10^{-15}$ – $10^{-10} M_{\odot}$ , which is particularly relevant for LISA through the associated SIGW signal. By shifting the enhancement scale of  $\mathcal{P}_{\mathcal{R}}(k)$ , PBHs can also form in other mass ranges, including the stellar-mass window relevant for LIGO-Virgo-KAGRA mergers.

In Fig. 7 we show the resulting PBH abundance for the benchmark potential (2.12). During radiation domination the predictions are non-robust because of their sensitivity to  $\delta_c$  and non-Gaussianities, whereas PBH formation in an early matter-dominated era is considerably more stable. By comparison, the associated SIGW spectrum, discussed below, retains more direct information about the shape of the primordial scalar power spectrum.

## 4.3 Scalar-induced stochastic gravitational waves

An approximately isotropic stochastic gravitational-wave background is conventionally characterized by the dimensionless energy density per logarithmic frequency interval,

$$\Omega_{\text{GW}}(f) \equiv \frac{1}{\rho_{\text{tot}}} \frac{d\rho_{\text{GW}}}{d \ln f}, \quad \rho_{\text{tot}} = \frac{3H_0^2}{8\pi G}. \quad (4.5)$$

In our scenario, strong scalar-induced gravitational waves are mainly produced when the enhanced scalar perturbations reenter the Hubble horizon. During radiation domination, the induced tensor spectrum can be computed within second-order cosmological perturbation theory [3, 4, 85–87]. The oscillation-averaged tensor power spectrum takes the form [86]

$$\overline{\mathcal{P}_h(\tau, k)} = \int_0^{\infty} dt \int_{-1}^1 ds \mathcal{T}(s, t, \tau, k) \mathcal{P}_{\mathcal{R}}\left(\frac{t+s+1}{2}k\right) \mathcal{P}_{\mathcal{R}}\left(\frac{t-s+1}{2}k\right), \quad (4.6)$$

where  $\mathcal{T}$  is a known kernel [86, 87]. The present-day GW energy density is then approximately

$$\Omega_{\text{GW}}(t_0, k) \simeq g_*^{-1/3} \frac{\Omega_{\gamma,0}}{24} \left( \frac{k}{aH} \right)^2 \overline{\mathcal{P}_h(k)}. \quad (4.7)$$

If horizon reentry occurs instead during an early matter-dominated era, density perturbations may become nonlinear prior to reheating, leading to qualitatively different GW spectra. In this case a dominant contribution can be estimated from gravitational radiation emitted during collapse and halo formation by the quadrupole moment  $\tilde{Q}_{ij}$  [88, 89]:

$$\Omega_{\text{GW}}(t_0, \omega_0) = \frac{1}{\rho_{\text{tot}}(t_0)} \int_{\mathcal{S}} d\alpha d\beta d\gamma \frac{1}{1+z_e} \frac{1}{V_k} \frac{4\pi G}{5c^5} \sum_{ij} \left| \tilde{Q}_{ij}(\omega) \right|^2 \omega^7 \mathcal{F}_D(\alpha, \beta, \gamma, \sigma), \quad (4.8)$$

where  $\mathcal{S}$  denotes the region leading to consistent nonspherical collapse,  $z_e$  is the emission redshift,  $V_k = 4\pi k^{-3}/3$  is the comoving horizon-entry volume, and  $\mathcal{F}_D$  is a probability density function.

Primordial non-Gaussianity can modulate both the amplitude and spectral shape of the induced signal [72]. However, unlike PBH formation, which is exponentially sensitive to the tail of the probability distribution, the SIGW amplitude is mainly determined by the scalar power spectrum. SIGWs therefore provide a comparatively robust probe of enhanced primordial fluctuations on small scales.

Large scalar perturbations associated with PBH production can generate signals as large as  $h^2 \Omega_{\text{GW}}(f_p) \gtrsim 10^{-14} - 10^{-12}$ , bringing them within reach of PTA experiments and future detectors such as LISA. In particular, multi-peak structures in  $\mathcal{P}_{\mathcal{R}}(k)$  are partially inherited by the GW spectrum, providing an observational window into the underlying inflationary dynamics.

Representative SIGW spectra for the benchmark potential (2.12) are shown in Fig. 7, including both radiation- and matter-dominated reentry scenarios, and compared with the frequency ranges probed by LISA and current PTA data [52, 54]. The parameters of the corresponding models are given in Table 1.

## 5 Conclusions and outlook

In this work we have presented a simple and generic mechanism to generate a strong enhancement of the primordial curvature power spectrum in two-field models of inflation. The key ingredient is a hierarchy of energy scales that gives rise to a two-stage inflationary evolution. During the transition between the two stages, the inflationary trajectory undergoes a sequence of sharp turns in field space, leading to an efficient transfer of power from entropic to adiabatic perturbations. This mechanism of “assisted enhancement” does not rely on fine-tuned inflection points, ultra-slow-roll phases, or specially engineered valleys in the potential. Instead, the mechanism can be realized within a simple setup consisting of quadratic potentials for each field, supplemented by a minimal interaction term. This is sufficient to generate a strong enhancement of the curvature power spectrum  $\mathcal{P}_{\mathcal{R}}(k)$  on small scales, while leaving the CMB scales unaffected by the amplification and free from significant non-Gaussian contributions.

The effects of turns and sharp features on the curvature perturbations can be understood in terms of localized departures from slow-roll, which act as transient sources for the curvature perturbation  $\mathcal{R}$  [37, 38]. When such events occur repeatedly and in close succession, their contributions can interfere constructively, leading to a resonant enhancement of the power

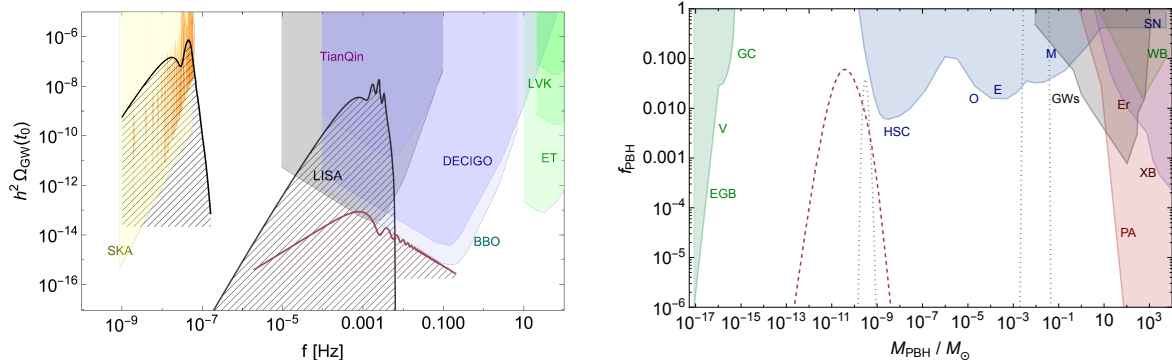


**Figure 7:** Left panel: Spectrum of scalar-induced GWs in our two-field scenario. The gray (dark-red) curve shows the signal produced during radiation domination (an early matter-dominated era), up to non-Gaussian corrections. Orange lines indicate PTA posteriors from NANOGrav, EPTA, and InPTA [53, 54]. Right panel: The corresponding PBH fractional abundance. The dotted gray (dashed dark-red) curve denotes PBHs formed during radiation domination (early matter domination). Shaded regions show current observational constraints. These PBH predictions are only indicative because of their sensitivity to non-Gaussian effects.

spectrum. The present work provides a concrete dynamical realization of this mechanism. The repeated turns naturally emerge from the oscillatory relaxation of one field during the transition between two stages of inflation, generating a sequence of localized pulses. As a result, the analytic intuition developed in the pulse approximation applies here, with the total enhancement controlled by the parameter  $W$  defined in (2.9), and the duration  $\Delta N$  of the turning phase, as discussed in Refs. [18, 38].

We illustrated the mechanism using a minimal two-field setup with canonical kinetic terms and a simple interaction potential (2.12). The first stage of inflation proceeds at a higher energy scale and sets the CMB normalization, while the second stage occurs at a lower scale. As the system relaxes from the first to the second stage, oscillatory motion in the heavier field induces repeated turns of the background trajectory, see Fig. 3. These turns act as transient sources for curvature perturbations, producing a localized amplification of the power spectrum over a narrow range of scales. Only modes that exit the horizon during the brief transition period are amplified, while both earlier and later modes remain unaffected. This naturally leads to a peaked primordial power spectrum, whose position and amplitude are controlled by the duration of the transition, the mass hierarchy, and the strength of the interaction between the fields. As a result, the curvature power spectrum can grow by several orders of magnitude at short scales while remaining consistent with the CMB at large scales.

It must be pointed out that our simple model employs only quadratic terms in the slow-roll phases. The effect on the scalar spectral index and the tensor-to-scalar ratio can be phenomenologically important. Modifications of the potential along the plateau of the first inflationary stage may be necessary in order to adjust such observables to the experimentally deduced values. However, the purpose of this work was to demonstrate a simple and generic mechanism for power-spectrum enhancement, rather than to construct a detailed inflationary model with perfect agreement with observations. We expect that this type of enhancement is broadly applicable in two- and multi-field inflation, and can arise for a broad range of

potential shapes.

The enhanced small scale curvature perturbations have direct implications for PBH formation. Modes that reenter the horizon during radiation domination with sufficiently large amplitude can collapse into PBHs. Moreover, an unavoidable and complementary prediction of this framework is the generation of a stochastic GW background induced at second order by scalar perturbations. The resulting scalar-induced gravitational wave (SIGW) background may be detectable by current and future GW experiments. We mention that our mechanism is expected to generate significant non-Gaussianity at short scales, which can substantially affect PBH abundance estimates and modify SIGW predictions beyond the simplest Gaussian treatment. A more detailed computation of the PBH abundance including non-Gaussian corrections, which are generically expected in turning trajectories, would refine the phenomenological predictions presented in this work. In any case, the possibility of observing non-Gaussianities of primordial fluctuations is very exciting, as it might provide information on the field content during inflation.

The localized nature of the power-spectrum enhancement, the possible peak structure inherited from the turning dynamics, and the correlation between PBH masses, GW frequencies and non-Gaussianities offer distinctive signatures that can be used to discriminate this scenario from single-field ultra-slow-roll or inflection-point models. The mechanism presented here highlights how seemingly generic features of multi-field dynamics can leave striking observable imprints on small-scale cosmological structures.

## References

- [1] Y. Akrami *et al.* [Planck], *Planck 2018 results. X. Constraints on inflation*, *Astron. Astrophys.* **641** (2020), A10.
- [2] S. Mollerach, D. Harari and S. Matarrese, *CMB polarization from secondary vector and tensor modes*, *Phys. Rev. D* **69** (2004), 063002.
- [3] K. N. Ananda, C. Clarkson and D. Wands, *The Cosmological gravitational wave background from primordial density perturbations*, *Phys. Rev. D* **75** (2007), 123518.
- [4] D. Baumann, P. J. Steinhardt, K. Takahashi and K. Ichiki, *Gravitational Wave Spectrum Induced by Primordial Scalar Perturbations*, *Phys. Rev. D* **76** (2007), 084019.
- [5] S. Hawking, *Gravitationally collapsed objects of very low mass*, *Mon. Not. Roy. Astron. Soc.* **152** (1971), 75.
- [6] B. J. Carr and S. W. Hawking, *Black holes in the early Universe*, *Mon. Not. Roy. Astron. Soc.* **168** (1974), 399-415.
- [7] B. Carr, K. Kohri, Y. Sendouda and J. Yokoyama, *Constraints on primordial black holes*, *Rept. Prog. Phys.* **84** (2021) no.11, 116902.
- [8] B. Carr and F. Kuhnel, *Primordial Black Holes*, [arXiv:2502.15279 [astro-ph.CO]].
- [9] D. Langlois, *Correlated adiabatic and isocurvature perturbations from double inflation*, *Phys. Rev. D* **59** (1999), 123512.
- [10] C. Gordon, D. Wands, B. A. Bassett and R. Maartens, *Adiabatic and entropy perturbations from inflation*, *Phys. Rev. D* **63** (2000), 023506.
- [11] S. Cremonini, Z. Lalak and K. Turzynski, *Strongly Coupled Perturbations in Two-Field Inflationary Models*, *JCAP* **03** (2011), 016.
- [12] X. Chen, *Primordial Features as Evidence for Inflation*, *JCAP* **01** (2012), 038.

- [13] S. Cespedes, V. Atal and G. A. Palma, *On the importance of heavy fields during inflation*, *JCAP* **05** (2012), 008.
- [14] A. Achúcarro, J. O. Gong, G. A. Palma and S. P. Patil, *Correlating features in the primordial spectra*, *Phys. Rev. D* **87** (2013) no.12, 121301.
- [15] M. Konieczka, R. H. Ribeiro and K. Turzyski, *The effects of a fast-turning trajectory in multiple-field inflation*, *JCAP* **07** (2014), 030.
- [16] A. Slosar, K. N. Abazajian, M. Abidi, P. Adshead, Z. Ahmed, D. Alonso, M. A. Amin, B. Ansarinejad, R. Armstrong and C. Baccigalupi, *et al. Scratches from the Past: Inflationary Archaeology through Features in the Power Spectrum of Primordial Fluctuations*, *Bull. Am. Astron. Soc.* **51** (2019) no.3, 98.
- [17] M. Braglia, D. K. Hazra, F. Finelli, G. F. Smoot, L. Sriramkumar and A. A. Starobinsky, *Generating PBHs and small-scale GWs in two-field models of inflation*, *JCAP* **08** (2020), 001.
- [18] J. Fumagalli, S. Renaux-Petel, J. W. Ronayne and L. T. Witkowski, *Turning in the landscape: A new mechanism for generating primordial black holes*, *Phys. Lett. B* **841** (2023), 137921.
- [19] J. Fumagalli, S. Renaux-Petel and L. T. Witkowski, *Oscillations in the stochastic gravitational wave background from sharp features and particle production during inflation*, *JCAP* **08** (2021), 030.
- [20] K. Inomata, E. McDonough and W. Hu, *Amplification of primordial perturbations from the rise or fall of the inflaton*, *JCAP* **02** (2022) no.02, 031.
- [21] A. A. Starobinsky and J. Yokoyama, *Density fluctuations in Brans-Dicke inflation*, [arXiv:gr-qc/9502002 [gr-qc]].
- [22] M. Sasaki and E. D. Stewart, *A General analytic formula for the spectral index of the density perturbations produced during inflation*, *Prog. Theor. Phys.* **95** (1996), 71-78.
- [23] J. Garcia-Bellido and D. Wands, *Metric perturbations in two field inflation*, *Phys. Rev. D* **53** (1996), 5437-5445.
- [24] A. D. Linde and V. F. Mukhanov, *Nongaussian isocurvature perturbations from inflation*, *Phys. Rev. D* **56** (1997), R535-R539.
- [25] A. Achúcarro, J. O. Gong, S. Hardeman, G. A. Palma and S. P. Patil, *Features of heavy physics in the CMB power spectrum*, *JCAP* **01** (2011), 030.
- [26] S. Pi, Y. l. Zhang, Q. G. Huang and M. Sasaki, *Scalaron from  $R^2$ -gravity as a heavy field*, *JCAP* **05** (2018), 042.
- [27] G. A. Palma, S. Sypsas and C. Zenteno, *Seeding primordial black holes in multifield inflation*, *Phys. Rev. Lett.* **125** (2020) no.12, 121301.
- [28] Y. Aldabergenov, A. Addazi and S. V. Ketov, *Primordial black holes from modified supergravity*, *Eur. Phys. J. C* **80** (2020) no.10, 917.
- [29] S. Kawai and J. Kim, *Primordial black holes and gravitational waves from nonminimally coupled supergravity inflation*, *Phys. Rev. D* **107** (2023) no.4, 043523.
- [30] P. Christodoulidis and J. O. Gong, *Enhanced power spectra from multi-field inflation*, *JCAP* **08** (2024), 062.
- [31] Y. Aldabergenov, D. Ding, W. Lin and Y. Wan, *Meso-inflationary Peccei–Quinn Symmetry Breaking with Nonminimal Coupling*, *Astrophys. J. Suppl.* **275** (2024) no.1, 14.
- [32] X. Wang, Y. l. Zhang and M. Sasaki, *Enhanced curvature perturbation and primordial black hole formation in two-stage inflation with a break*, *JCAP* **07** (2024), 076.
- [33] J. Kim, X. Wang, Y. l. Zhang and Z. Ren, *Enhancement of primordial curvature perturbations in  $R^3$ -corrected Starobinsky-Higgs inflation*, *JCAP* **09** (2025), 011.

- [34] R. Gonzalez Quaglia, M. Michelotti, D. Roest, J. J. Carrasco, R. Kallosh and A. Linde, *Post-inflationary enhancement of adiabatic perturbations in modular cosmology*, *JCAP* **10** (2025), 045.
- [35] D. L. Lorenzoni, S. R. Geller, D. I. Kaiser and E. McDonough, *Primordial Black Holes from Inflation with a Spectator Field*, [arXiv:2512.04199 [astro-ph.CO]].
- [36] K. Kefala, G. P. Kodaxis, I. D. Stamou and N. Tetradis, *Features of the inflaton potential and the power spectrum of cosmological perturbations*, *Phys. Rev. D* **104** (2021) no.2, 023506.
- [37] I. Dalianis, G. P. Kodaxis, I. D. Stamou, N. Tetradis and A. Tsigkas-Kouvelis, *Spectrum oscillations from features in the potential of single-field inflation*, *Phys. Rev. D* **104** (2021) no.10, 103510.
- [38] K. Boutivas, I. Dalianis, G. P. Kodaxis and N. Tetradis, *The effect of multiple features on the power spectrum in two-field inflation*, *JCAP* **08** (2022) no.08, 021.
- [39] I. Dalianis, *Features in the Inflaton Potential and the Spectrum of Cosmological Perturbations*, [arXiv:2310.11581 [astro-ph.CO]].
- [40] A. Katsis, *The sinusoidal valley: a recipe for high peaks in the scalar and induced tensor spectra*, *JCAP* **06** (2025), 010.
- [41] A. Achucarro, J. O. Gong, S. Hardeman, G. A. Palma and S. P. Patil, *Effective theories of single field inflation when heavy fields matter*, *JHEP* **05** (2012), 066.
- [42] D. Polarski and A. A. Starobinsky, *Isocurvature perturbations in multiple inflationary models*, *Phys. Rev. D* **50** (1994), 6123-6129.
- [43] V. F. Mukhanov and P. J. Steinhardt, *Density perturbations in multifield inflationary models*, *Phys. Lett. B* **422** (1998), 52-60.
- [44] S. Garcia-Saenz, S. Renaux-Petel and J. Ronayne, *Primordial fluctuations and non-Gaussianities in sidetracked inflation*, *JCAP* **07** (2018) 057.
- [45] A. B. Lahanas and D. V. Nanopoulos, *The Road to No Scale Supergravity*, *Phys. Rept.* **145** (1987), 1.
- [46] J. Ellis, D. V. Nanopoulos and K. A. Olive, *No-Scale Supergravity Realization of the Starobinsky Model of Inflation*, *Phys. Rev. Lett.* **111** (2013), 111301.
- [47] R. Kallosh and A. Linde, *Multi-field Conformal Cosmological Attractors*, *JCAP* **12** (2013), 006.
- [48] R. Kallosh and A. Linde, *Non-minimal Inflationary Attractors*, *JCAP* **10** (2013), 033.
- [49] J. Garcia-Bellido, J. Rubio, M. Shaposhnikov and D. Zenhausern, *Higgs-Dilaton Cosmology: From the Early to the Late Universe*, *Phys. Rev. D* **84** (2011), 123504.
- [50] D. I. Kaiser and E. I. Sfakianakis, *Multifield Inflation after Planck: The Case for Nonminimal Couplings*, *Phys. Rev. Lett.* **112** (2014) no.1, 011302.
- [51] Y. Ema, *Higgs Scalaron Mixed Inflation*, *Phys. Lett. B* **770** (2017), 403-411.
- [52] G. Agazie et al. [NANOGrav], *The NANOGrav 15 yr Data Set: Evidence for a Gravitational-wave Background*, *Astrophys. J. Lett.* **951** (2023) no.1, L8.
- [53] A. Afzal et al. [NANOGrav], *The NANOGrav 15 yr Data Set: Search for Signals from New Physics*, *Astrophys. J. Lett.* **951** (2023) no.1, L11; erratum: *Astrophys. J. Lett.* **971** (2024) no.1, L27; erratum: *Astrophys. J.* **971** (2024) no.1, L27].
- [54] J. Antoniadis et al. [EPTA and InPTA:], *The second data release from the European Pulsar Timing Array - III. Search for gravitational wave signals*, *Astron. Astrophys.* **678** (2023), A50.
- [55] D. J. Reardon, A. Zic, R. M. Shannon, G. B. Hobbs, M. Bailes, V. Di Marco, A. Kapur, A. F. Rogers, E. Thrane and J. Askew, et al. *Search for an Isotropic Gravitational-wave Background with the Parkes Pulsar Timing Array*, *Astrophys. J. Lett.* **951** (2023) no.1, L6.

- [56] H. Xu, S. Chen, Y. Guo, J. Jiang, B. Wang, J. Xu, Z. Xue, R. N. Caballero, J. Yuan and Y. Xu, *et al. Searching for the Nano-Hertz Stochastic Gravitational Wave Background with the Chinese Pulsar Timing Array Data Release I*, *Res. Astron. Astrophys.* **23** (2023) no.7, 075024.
- [57] P. Amaro-Seoane *et al.* [LISA], *Laser Interferometer Space Antenna*, [arXiv:1702.00786 [astro-ph.IM]].
- [58] A. Abac *et al.* [ET], *The Science of the Einstein Telescope*, [arXiv:2503.12263 [gr-qc]].
- [59] C. Caprini and D. G. Figueroa, *Cosmological Backgrounds of Gravitational Waves*, *Class. Quant. Grav.* **35** (2018) no.16, 163001.
- [60] M. C. Guzzetti, N. Bartolo, M. Liguori and S. Matarrese, *Gravitational waves from inflation*, *Riv. Nuovo Cim.* **39** (2016) no.9, 399-495.
- [61] S. Young, C. T. Byrnes and M. Sasaki, *Calculating the mass fraction of primordial black holes*, *JCAP* **07** (2014), 045.
- [62] O. Özsoy, *Inflation and Primordial Black Holes*, *Universe* **9** (2023) 203.
- [63] D. G. Figueroa, M. Pieroni, A. Ricciardone and P. Simakachorn, *Cosmological Background Interpretation of Pulsar Timing Array Data*, *Phys. Rev. Lett.* **132** (2024) no.17, 171002.
- [64] S. Balaji, G. Domenech and J. Silk, *Induced gravitational waves from slow-roll inflation after an enhancing phase*, *JCAP* **09** (2022), 016.
- [65] S. Balaji, G. Domènech and G. Franciolini, *Scalar-induced gravitational wave interpretation of PTA data: the role of scalar fluctuation propagation speed*, *JCAP* **10** (2023), 041.
- [66] B. Carr and F. Kuhnel, *Primordial black holes as dark matter candidates*, *SciPost Phys. Lect. Notes* **48** (2022), 1.
- [67] B. Carr, S. Clesse, J. Garcia-Bellido, M. Hawkins and F. Kuhnel, *Observational evidence for primordial black holes: A positivist perspective*, *Phys. Rept.* **1054** (2024), 1-68.
- [68] X. Chen, *Primordial Non-Gaussianities from Inflation Models*, *Adv. Astron.* **2010** (2010), 638979.
- [69] Y. Akrami *et al.* [Planck], *Planck 2018 results. IX. Constraints on primordial non-Gaussianity*, *Astron. Astrophys.* **641** (2020), A9.
- [70] C. T. Byrnes, E. J. Copeland and A. M. Green, *Primordial black holes as a tool for constraining non-Gaussianity*, *Phys. Rev. D* **86** (2012), 043512.
- [71] S. Young and C. T. Byrnes, *Primordial black holes in non-Gaussian regimes*, *JCAP* **08** (2013), 052.
- [72] R. g. Cai, S. Pi and M. Sasaki, *Gravitational Waves Induced by non-Gaussian Scalar Perturbations*, *Phys. Rev. Lett.* **122** (2019) no.20, 201101.
- [73] B. J. Carr, *The Primordial black hole mass spectrum*, *Astrophys. J.* **201** (1975), 1-19.
- [74] J. C. Niemeyer and K. Jedamzik, *Near-critical gravitational collapse and the initial mass function of primordial black holes*, *Phys. Rev. Lett.* **80** (1998), 5481-5484.
- [75] I. Musco and J. C. Miller, *Primordial black hole formation in the early universe: critical behaviour and self-similarity*, *Class. Quant. Grav.* **30** (2013), 145009.
- [76] T. Harada, C. M. Yoo and K. Kohri, *Threshold of primordial black hole formation*, *Phys. Rev. D* **88** (2013) no.8, 084051; *erratum: Phys. Rev. D* **89** (2014) no.2, 029903.
- [77] G. Franciolini, A. Kehagias, S. Matarrese and A. Riotto, *Primordial Black Holes from Inflation and non-Gaussianity*, *JCAP* **03** (2018), 016.
- [78] V. Atal and C. Germani, *The role of non-gaussianities in Primordial Black Hole formation*, *Phys. Dark Univ.* **24** (2019), 100275.

- [79] V. De Luca, G. Franciolini, A. Kehagias, M. Peloso, A. Riotto and C. Ünal, *The Ineludible non-Gaussianity of the Primordial Black Hole Abundance*, *JCAP* **07** (2019), 048
- [80] H. Firouzjahi and A. Riotto, *Sign of non-Gaussianity and the primordial black holes abundance*, *Phys. Rev. D* **108** (2023) no.12, 123504
- [81] T. Harada, C. M. Yoo, K. Kohri, K. i. Nakao and S. Jhingan, *Primordial black hole formation in the matter-dominated phase of the Universe*, *Astrophys. J.* **833** (2016) no.1, 61.
- [82] T. Harada, C. M. Yoo, K. Kohri and K. I. Nakao, *Spins of primordial black holes formed in the matter-dominated phase of the Universe*, *Phys. Rev. D* **96** (2017) no.8, 083517; erratum: *Phys. Rev. D* **99** (2019) no.6, 069904.
- [83] B. Carr and F. Kuhnel, *Primordial Black Holes as Dark Matter: Recent Developments*, *Ann. Rev. Nucl. Part. Sci.* **70** (2020), 355-394.
- [84] A. M. Green, *Primordial black holes as a dark matter candidate - a brief overview*, *Nucl. Phys. B* **1003** (2024), 116494.
- [85] J. R. Espinosa, D. Racco and A. Riotto, “A Cosmological Signature of the SM Higgs Instability: Gravitational Waves,” *JCAP* **09** (2018), 012.
- [86] K. Kohri and T. Terada, *Semianalytic calculation of gravitational wave spectrum nonlinearly induced from primordial curvature perturbations*, *Phys. Rev. D* **97** (2018) no.12, 123532.
- [87] G. Domènech, *Scalar Induced Gravitational Waves Review*, *Universe* **7** (2021) no.11, 398.
- [88] I. Dalianis and C. Kouvaris, *Gravitational waves from density perturbations in an early matter domination era*, *JCAP* **07** (2021), 046.
- [89] I. Dalianis and C. Kouvaris, *Gravitational waves from collapse of pressureless matter in the early universe*, *JCAP* **10** (2024), 006.